Acta Cryst. (1979). B**35**, 1937–1944

The Crystallographic Analysis of $InMn_3$, a New Form of γ-Brass Structure with a *P* Cell

By J. K. Brandon, Hwang Su Kim and W. B. Pearson

Department of Physics, University of Waterloo, Waterloo, Ontario, Canada N2L 3G1

(*Received* 2 *January* 1979; *accepted* 9 *April* 1979)

Abstract

Single-crystal X-ray diffraction experiments have shown that the alloy of composition $InMn_3$ has a γ-brass-type structure with space group $P\bar{4}3m$ and room-temperature cubic cell constant $a = 9{\cdot}420 \pm 0{\cdot}004$ Å. At the relatively large atomic-radius ratio $R_{In}/R_{Mn} \simeq 1{\cdot}3$ the In atoms occupy nearly completely the cubo-octahedral (*CO*) sites of one of the two clusters of 26 atoms which make up the 52-atom primitive unit cell (*P* cell). In atoms also partially occupy the octahedral (*OH*) sites of the same cluster. This distribution of the large and small constituent atoms represents a newly discovered type of atomic ordering for *P*-cell γ-brass structures, which gives an improved packing fraction for a large radius ratio when the larger In atoms order in *OH* and *CO* sites rather than inner tetrahedral (*IT*) and *CO* sites, and furthermore the ordering in a *P* cell reduces the number of In–In contacts. Previously published powder intensity data for the high-temperature γ-Cu–In phase, which also has a relatively large radius ratio of $R_{In}/R_{Cu} \simeq 1{\cdot}3$, is shown to be consistent with calculations for a model structure with a *P* cell and with large In and small Cu atoms adopting the $InMn_3$ type of ordering.

Introduction

Our previous work on γ-brasses has led to an understanding of why certain γ-phase alloys stabilize with ~9 Å cubic body-centred (*I*) Bravais lattices, others with ~9 Å cubic primitive (*P*) lattices, some with ~18 Å cubic face-centred (*F*) lattices and a few with rhombohedral (*R*) lattices derived from the cubic form. Among each of these varieties, we have examined various factors which affect the atomic ordering and structural stability (Pearson, Brandon & Brizard, 1976; Booth, Brandon, Brizard, Chieh & Pearson, 1977; Brandon, Brizard, Pearson & Tozer, 1977; Brandon, Pearson, Riley, Chieh & Stokhuyzen, 1977). These previous studies led to predictions of the atomic ordering in γ-$InMn_3$ and γ-Cu–In where the radius ratios are very disparate ($R_{In}/R_{Mn} \simeq 1{\cdot}3$).

Previous X-ray investigations of these two phases by powder diffraction methods [Zwicker (1950) and Aoyagi & Sugihara (1962) on γ-$InMn_3$; Reynolds (1952) on γ-Cu–In] identified them as γ-brass-type structures but provided no information about their lattice types, their space groups, or their atomic ordering.

The unique ordering in a *P* cell which we report here for our single-crystal work on $InMn_3$ prompted our attempts to see how well a similar *P*-cell ordering model would fit the high-temperature γ-Cu–In powder diffraction data of Reynolds (1952).

Experimental

Appropriate amounts of 99·999% pure In (supplied by A. D. Mackay Ltd) and spectroscopically pure Mn (supplied by Johnson Matthey Chemicals Ltd) were used to prepare a mixture with 41·06 wt% In. The mixture was evacuated in a quartz tube to 4×10^{-4} Pa; the tube was sealed, and the sample was heated to 823 K for 3 h to allow molten In to completely mix with the Mn. The sample was annealed for 20 d at 1093 ± 10 K, and rapidly quenched to room temperature in a water bath. By using this method it was expected from the In–Mn phase diagram (Hansen, 1958) that a mixed alloy containing phases $InMn_3$ and In would result, from which one might obtain $InMn_3$ single crystals. The resulting ingot was black on its outer surface, but when broken it was found to be hollow with bright silver-coloured crystals on the inner surfaces. Portions of the inner part of the sample were fragmented for use in powder X-ray diffraction investigations and in a search for $InMn_3$ single crystals. Other portions of the ingot were studied later by powder diffraction to check for the presence of any other phases (Kim, 1979).

The powder diffraction patterns of material from the inner part of the ingot could be indexed as a mixture of In and a cubic material with the known cell constant of $InMn_3$. Small fragments were then selected from the sample and a single crystal of $InMn_3$ was detected by inspection of Weissenberg and precession diffraction photographs. Zero- and upper-level Weissenberg

0567-7408/79/091937-08$01.00

photographs were indexed on the basis of a cubic cell with approximate cell constant 9·42 Å and with [$\bar{1}$10] as rotation axis (Ni-filtered Cu $K\bar{\alpha}$ radiation, λ = 1·54178 Å). These measurements confirmed that $InMn_3$ had been obtained since there was reasonable agreement with previously reported cubic cell constants for this phase (9·44 Å, Aoyagi & Sugihara, 1962; 9·43 Å, Zwicker, 1950). Of immediate interest from the single-crystal diffraction photographs was the observation of weak but easily visible reflections of type $h + k + l$ = odd, indicating that $InMn_3$ has a primitive (P) cubic lattice rather than the body-centred (I) lattice of the archetype Cu_5Zn_8 γ-brass structure.

The single-crystal diffraction patterns also showed the intensity relationships of Laue symmetry class $m3m$ with no systematically absent reflections, allowing possible space groups $P432$ (No. 207), $P\bar{4}3m$ (No. 215) and $Pm3m$ (No. 221) (*International Tables for X-ray Crystallography*, 1969). The likely space group was taken as $P\bar{4}3m$ subject to confirmation by structure analysis.

Cell-constant and relative-intensity measurements were made using a General Electric XRD-6 single-crystal automated diffractometer equipped with a scintillation counter and a pulse-height analyser. The sample was aligned with [$\bar{1}$10] along the φ axis of the diffractometer and the cell constant was refined by a least-squares fit to the measured 2θ values of 10 reflections (Zr-filtered Mo $K\bar{\alpha}$ radiation, λ = 0·71069 Å). The same diffractometer and radiation were used in a θ–2θ scan mode to collect relative intensity data. A scan speed of 2° min^{-1} and a scan range in 2θ of (1·80 + 0·86 tan θ)° were used, with 10 s background measurements taken at the beginning and end of each scan. Several reflections were measured as standards and were repeated every 100 reflections to check uniform conditions of the crystal and X-ray source. 2129 reflections with 2θ < 70° (Mo $K\bar{\alpha}$ radiation) in the first octant were measured.

Table 1. *Crystal data for* $InMn_3$

Crystal system	Cubic
Space group	$P\bar{4}3m$ (T_d^1, No. 215)
Cell constant, a (Å) (293 K)	9·420 ± 0·004
Cell volume, V (Å^3)	835·9 ± 1·1
Measured density, D_m (Mg m^{-3})	7·11 ± 0·32*
Atoms per unit cell, N	51·2 ± 2·3†
Calculated density for N = 52, D_x (Mg m^{-3})	7·22
Absorption coefficient (Mo $K\bar{\alpha}$) (mm^{-1})	23·44

* This density measurement and standard deviation come from numerous attempts on different samples taken from the central portions of the ingot. Powder photographs have shown that such samples would contain a mixture of phases.

† This N value is calculated using the measured D_m and a values assuming the composition $InMn_3$. The refined model contains N = 52 atoms as for the archetype γ-brass and D_x refers to this 52-atom model at the same composition.

The data were corrected for absorption using a locally modified version of the program *NRC*-3 (originally written by F. R. Ahmed and P. Singh, Ottawa) run on the University of Waterloo IBM 360 Model 75 computer. The sample volume was approximately 1·87 × 10^{-3} mm^3. The linear absorption coefficient and other crystal data are summarized in Table 1.

The 2129 reflections were next corrected for background, Lorentz, and polarization effects and symmetry-equivalent reflections were averaged using the program *DATAPREP*. There remained 428 independent intensities, of which 6 were negative and were either treated as zero or excluded from the later refinements. Errors from counting statistics and from background corrections were combined to derive standard deviations in each intensity value.

Solving and refining the structure

Since a structure related to that of other γ-brass phases was expected, a trial set of atomic coordinates was derived based on the cluster model for γ phases. In this model, clusters of 26 atoms each with $\bar{4}3m$ symmetry pack together as pseudo-atoms in a body-centred cubic arrangement. For γ-brasses with the body-centred cubic lattice (I cell), two crystallographically identical clusters occur per unit cell of edge ~9 Å. γ-Brasses with the ~9 Å P cell are composed of two different clusters, A and B, centred respectively at 000 and $\frac{111}{222}$ in the cubic cell. Each 26-atom cluster is composed of: (*a*) 4 atoms usually in contact comprising an inner tetrahedron (IT); (*b*) 4 atoms forming an outer tetrahedron (OT) such that each OT atom is usually in contact with 3 IT atoms; (*c*) 6 atoms forming an octahedron (OH) such that each OH atom is close to 2 IT and 2 OT atoms; and (*d*) 12 atoms forming a cuboctahedron (CO) such that each CO atom is close to 1 IT, 1 OT, 2 OH and 2 CO atoms. By using this basic arrangement approximate coordinates can be generated for a starting-model structure.

Various models for atomic ordering of In and Mn among the eight possible P-cell crystallographic sites were proposed and tested. Some models were based on previously known P-cell γ phases such as Al_4Cu_9 where the larger atomic species occupy IT sites of the A cluster and CO sites of the B cluster. Other models were attempted with ordering schemes arising from predictions based on packing fractions and other concepts. These models had large In atoms primarily on OH and CO sites. In addition, because of possible variations from the expected $InMn_3$ composition, several models were attempted with slight composition changes. For example, Aoyagi & Sugihara (1962) reported a narrow single-phase field near $InMn_3$ and our own density measurements could easily allow

variations between the compositions $In_{12}Mn_{40}$ (23·07 at.% In, $D_x \simeq 7{\cdot}10$ Mg m^{-3}) and $In_{14}Mn_{38}$ (26·90 at.% In, $D_x \simeq 7{\cdot}34$ Mg m^{-3}).

All trial models were refined using the full-matrix crystallographic least-squares program *LSTSQR*. Scattering factors for In and Mn based on the Thomas–Fermi–Dirac statistical model and corrections for anomalous scattering with Mo $K\bar{\alpha}$ radiation were taken from *International Tables for X-ray Crystallography* (1968). The least-squares program refined the scale factor, extinction-correction parameter, atomic coordinates and individual isotropic temperature factors for each atom. The function minimized was $\sum w(|F_o| - |F_c|)^2$. All 422 reflections were used with unit weights ($w = 1$) for the initial tests of model structures.

Table 2 shows results for a few ordering models of particular interest. Model 1, which resembles the *P*-cell ordering of Al_4Cu_9 with the available large In atoms in *AIT* and *BCO*, is not appropriate because of its large R_w and large resulting temperature factor for *AIT* $\{R_w \equiv [\sum w(|F_o| - |F_c|)^2/\sum w|F_o|^2]^{1/2}$, summations over all reflections$\}$. Model 5 which uses only the *BCO* sites for large In atoms refined to a more reasonable R_w value than did model 1, and final temperature factors in model 5 suggested possible improvements by placing fewer In atoms in *BCO* and adding some In atoms to *BOH*. Model 12 with In only in *CO* sites (but with different proportions in *ACO* and *BCO* to give a *P* cell) had a promising R_w value perhaps because of similarity to model 5 with large In concentration in *BCO*, but the fact that *ACO* had the largest isotropic temperature factor (*B*) led us to believe that *CO* sites in the second cluster could not actually accommodate much In. Here again, as in model 5, the *B* value of the *BOH* site remained the smallest. Model 2 has been included in the table to show the results typical of models where an appreciable fraction of the In atoms are removed from the *BCO* site. In this case with the remaining In atoms placed in *AOH* the refinement has adjusted for an excess of electrons by the large increase in the temperature factor *B* of *AOH*. The large R_w value of 0·205 is typical of models without a nearly complete In occupancy of *BCO* and such models are far poorer.

From these results for trial models, the main features of atomic ordering were deduced and further refinement was made based on minor changes to model 5 (for example, models 9, 8, 11, 6 and 14). Each model gave very similar coordinates for the atoms. The calculated structure factors showed three reflections with poor agreement between F_o and F_c for all models. Inspection of the raw diffractometer data for these

Table 2. *Results of some trial ordering models for* $InMn_3$

Model No.	Composition ratio In:Mn	Numbers of In atoms in *A IT/OT/OH/CO* *B IT/OT/OH/CO**	R_w†	Comments
1	13:39	4/0/0/0 0/0/0/9	0·139	*B* of *AIT* increased to ~4·0 Å^2 indicating unsuitable choice of In in *AIT*. Model resembles Al_4Cu_9-type atomic ordering.
5	12:40	0/0/0/0 0/0/0/12	0·103	Model resembles Al_4Cu_9 ordering without any large In atoms in *AIT*. *B* of *BOH* was considerably smaller (0·26 Å^2) than for other sites, and *B BCO* had the largest value (1·3 Å^2).
12	12:40	0/0/0/2 0/0/0/10	0·115	Model shares In between *ACO* and *BCO*. *B* of *ACO* becomes largest of any site. *B* of *BOH* remains the smallest.
2	12:40	0/0/6/0 0/0/0/6	0·205	Example of model with relatively small occupation of *BCO* by In and with remaining In placed in *AOH*. *B* of *AOH* increased to 4·8 Å^2.
9	13:39	0/0/0/0 0/0/1/12	0·092	
8	14:38	0/0/0/0 0/0/2/12	0·084	*B* of *BOH* and *BCO* became the largest values suggesting perhaps too much In, consistent with an In stoichiometry higher than expected.
11	13:39	0/0/0/0 0/0/2/11	0·086	
6	13:39	0/0/0/0 0/0/3/10	0·087	
14	12:40	0/0/0/0 0/0/2/10	0·089	

* The remainder of the sites contain Mn to make up a 52-atom unit cell.
† Unit weights were used; all 422 reflections were included.

Table 3. *Structural data for* $InMn_3$ (*anisotropic temperature factor refinement*, $R_w = 0{\cdot}044$)

Figures in parentheses are standard errors in the last digits quoted as derived in the least-squares refinement.

Cluster and site	Point set		x	z	B (Å^2) or β_{11}	β_{22}	β_{33}	β_{12} (×10^4)	β_{13}	β_{23}
AIT	4(*e*) *xxx*	4 Mn	0·0953 (3)		0·86 (5)					
BIT	4(*e*) *xxx*	4 Mn	0·5975 (3)		0·90 (5)					
AOT	4(*e*) *xxx*	4 Mn	−0·1595 (3)		0·70 (5)					
BOT	4(*e*) *xxx*	4 Mn	0·3380 (3)		0·75 (5)					
AOH	6(*f*) 00*z*	6 Mn	0	0·3390 (4)	22 (3)	22	29 (3)	4 (2)	0	0
BOH	6(*g*) $\frac{11}{22}z$	4 Mn + 2In	0·5	0·8609 (3)	26 (2)	26	50 (3)	6 (2)	0	0
ACO	12(*i*) *xxz*	12 Mn	0·2868 (2)	0·0636 (3)	31 (2)	31	33 (2)	−3 (2)	−5 (2)	−5
BCO	12(*i*) *xxz*	1 Mn + 11In	0·8124 (1)	0·5455 (1)	42 (1)	42	21 (1)	−18 (1)	−5 (1)	−5

Table 4. *Principal axes of the ellipsoids of thermal motion as calculated from the OH and CO anisotropic temperature factors*

Site	Root-mean-square displacements along principal axes (Å)	Directions* of principal axes with respect to cell axes *a*,*b*,*c* (°)		
AOH	0·1139	90	90	0
00*z*	0·1070	45	45	90
	0·0907	45	135	90
ACO	0·1318	66·25	66·25	145·29
xxz	0·1232	45	135	90
	0·1009	54·46	54·46	55·29
BOH	0·1493	90	90	0
$\frac{11}{22}z$	0·1212	45	45	90
	0·0950	45	135	90
BCO	0·1643	45	135	90
xxz	0·1151	55·80	55·80	127·35
	0·0837	64·60	65·60	37·35

* The directions of all principal axes in the *OH* sites are fixed by symmetry constraints. In the *CO* sites, the direction of one principal axis is constrained.

Table 5. *Observed and calculated structure factors for* $InMn_3$

The six F_o assigned to be zero and the three marked with an asterisk were not included in the refinement for reasons given in the text. For the remaining 419 reflections $R_w = 0{\cdot}044$ (unit weights) using the model parameters quoted in Table 3.

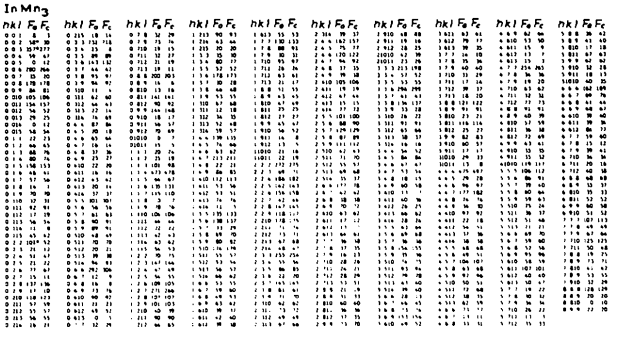

three reflections showed large background variations over their scan ranges. These three reflections, 002, 003, and 022, were therefore considered to be unreliable and they were removed from further refinement, leaving 419 reflections. Refinements using unit weights and isotropic temperature parameters led to R_w values of 0·071 for model 6, 0·073 for 11, 0·074 for 14, and 0·077 for 8. A detailed survey with changes in steps of one In atom on *BOH* and *BCO* left models 6 and 11 as favoured.

Anisotropic temperature factors* were then introduced, since it has been pointed out that significant anisotropic thermal motions of *OH* and *CO* atoms may exist in γ-brass structures (Brandon, Brizard, Chieh, McMillan & Pearson, 1974). Model 11 with anisotropic temperature factors for *AOH*, *ACO*, *BOH* and *BCO* sites emerged as the favoured model. R_w was 0·044 for 419 reflections and unit weights. This may be compared to the isotropic model which had refined to $R_w = 0{\cdot}073$ with unit weights.

Table 3 gives the refined parameters for the final model. Table 4 gives an analysis of the principal axis magnitudes and directions for the anisotropic thermal parameters. The observed and calculated structure factors are in Table 5. Table 6 lists the coordination polyhedra for atoms in each crystallographic site with the interatomic distances.

Discussion

(*a*) *The P cell and the new type of* γ-*brass atomic ordering for* $InMn_3$

These single-crystal diffraction experiments have shown that $InMn_3$ has a γ-brass-type arrangement of atoms with a *P* cell. This *P* cell was apparently not evident in the two previous powder diffraction studies, and the importance of applying single-crystal methods

* The form of the anisotropic temperature factor for each atom is $T = \exp[-(\beta_{11}h^2 + \beta_{22}k^2 + \beta_{33}l^2 + 2\beta_{12}hk + 2\beta_{23}kl + 2\beta_{13}hl)]$.

in our current analyses of γ-brass-type phases is stressed.

Compared to previously known *P*-cell γ-brasses such as Cu_9Al_4 (von Heidenstam, Johansson & Westman, 1968; Westman, 1965; Arnberg & Westman, 1978) and γ_1-Cu_9Ga_4 (Stokhuyzen, Brandon, Chieh & Pearson, 1974), the atomic ordering in $InMn_3$ is unique. Whereas the Cu_9Al_4 *P*-cell structure has its larger Al atoms at a composition of 30·8 at.% ordered in *BCO* and *AIT*, $InMn_3$ has its large In atoms at a composition of 25·0 at.% ordered predominantly in *BCO* and partially in *BOH*. Why these two different ordering schemes would occur among *P*-cell γ-brass structures can be understood in terms of packing efficiencies at the respective radius ratios of the two elements and in terms of maximizing the number of In–Mn neighbours while minimizing the number of In–In neighbours in the structure. [Details are presented below in (*c*).]

(*b*) *Interatomic distances and compulsory contacts in* $InMn_3$

Table 6 shows that interatomic distances involving *BCO* are generally larger because of the occupancy of this site by larger In atoms. The same is true to some extent for *BOH* which was found to have a mixed occupancy by In and Mn atoms. These observed distances are therefore compatible with the atomic ordering.

Owing to the unique ordering and large relative size differences of atoms in $InMn_3$, those contacts between atoms on different site sets which are compressed are somewhat different from those in other γ-brasses (Brandon, Brizard, Pearson & Tozer, 1977), as Table 6 shows. In contrast to the *I*-cell γ-brasses and other *P*-cell examples with radius ratios closer to unity, the *A* clusters in $InMn_3$ do not contact each other along $\langle 100 \rangle$, as shown by the distinct lack of any compressions in *AOH–AOH'* distances. Whereas the *AOH* atom at 00*z* has two close *BCO* neighbours along $\pm[1\bar{1}0]$ in a plane perpendicular to [001], it is relatively free of close contacts along [001] and somewhat free along $\pm[110]$ (these directions are specified with respect to an origin at the *AOH* atom). Hence we can understand the observed directions of the major and minor principal axes of the *AOH* anisotropic temperature factor (see Table 4). At first sight, the *BOH–BOH'* compressed contact would seem to be the result of interactions between two *B* clusters along $\langle 100 \rangle$-type directions. However, the fact that *BOH* does not have close contact with either *BIT* or *BOT* suggests that the pressure is not transferred into the core of the *B* cluster, and the *BOH* atom at $\frac{11}{22}z$ may be relatively free to move along $-[001]$, constrained only by the *BOH'* atom along $+[001]$ and four *BCO* atoms in a plane perpendicular to [001]. When *BOH* is statistically occupied by a smaller Mn atom, the *BOH–BOH'* atom is not in compression; when *BOH* is statistically occupied by a larger In atom, the In atom could sit closer to the centre of the *B* cluster and contact *BIT* and *BOT* atoms. These ideas explain why the anisotropic thermal ellipsoid of the *BOH* atom at $\frac{11}{22}z$ has its major principal axis along [001], and they also suggest how the *BOH* site might be an appropriate one in the $InMn_3$ structure to accommodate a mixture of In and Mn atoms, perhaps even at the expense of completely filling *BCO* with the available In atoms at this composition.

Table 6. *Interatomic distances* (Å) *in* $InMn_3$ *for the coordination shells about each atom*

Numbers in parentheses are deviations from hard-sphere CN 12 radii sums.

A primed atom symbol is used to indicate a contact to an atom in a neighbouring cluster where this distinction is not obvious from the *A* and *B* cluster designation. Estimated standard errors are ~0·03 Å.

	Cluster *A*			Cluster *B*		
Number	*AIT* (Mn) to			*BIT* (Mn) to		
3	*AIT*	2·54	(−0·03)	*BIT*	2·60	(0·03)
3	*AOT*	2·55	(−0·02)	*BOT*	2·59	(0·02)
3	*AOH*	2·62	(0·05)	*BOH*	2·80	(0·11)
3	*ACO*	2·57	(0·00)	*BCO*	2·91	(−0·01)
	AOT (Mn) to			*BOT* (Mn) to		
3	*AIT*	2·55	(−0·02)	*BIT*	2·59	(0·02)
3	*AOH*	2·72	(0·15)	*BOH*	2·86	(0·17)
3	*ACO*	2·70	(0·13)	*BCO*	2·80	(−0·12)
3	*BCO*	2·80	(−0·12)	*ACO*	2·67	(0·10)
	AOH (Mn) to			*BOH* ($\frac{2}{3}$Mn + $\frac{1}{3}$In) [Mn+]		
2	*AIT*	2·62	(0·05)	*BIT*	2·80	(0·11)
2	*AOT*	2·72	(0·15)	*BOT*	2·86	(0·17)
1	*AOH'*	3·03	(0·34)	*BOH'*	2·62	(−0·20)
4	*ACO*	2·81	(0·24)	*BCO*	3·01	(−0·03)
2	*BCO*	2·73	(−0·19)	*ACO*	2·93	(0·14)
2	*BCO*	3·17	(0·25)	*ACO*	3·42	(0·73)
	ACO (Mn) to			*BCO* ($\frac{1}{12}$Mn + $\frac{11}{12}$In) [In+]		
1	*AIT*	2·57	(0·00)	*BIT*	2·91	(−0·01)
1	*AOT*	2·70	(0·13)	*BOT*	2·80	(−0·12)
1	*BOT*	2·67	(0·10)	*AOT*	2·80	(−0·12)
2	*AOH*	2·81	(0·24)	*BOH*	3·01	(−0·03)
1	*BOH*	2·93	(0·24)	*AOH*	2·73	(−0·19)
1	*BOH*	3·42	(0·73)	*AOH*	3·17	(0·25)
2	*ACO*	2·97	(0·30)	*BCO*	3·56	(0·30)
2	*BCO*	2·86	(−0·06)	*ACO*	2·99	(0·07)
2	*BCO*	2·99	(0·07)	*ACO*	2·86	(−0·06)
2	*ACO'*	4·19	(1·62)	*BCO'*	3·64	(0·38)

(*c*) *Reasons for stability of* $InMn_3$ *with the observed P cell and atomic ordering*

Our previous predictions, that the packing fraction would be dominant and that it would control the ordering of the atoms at a radius ratio as disparate as 1·3, were based on an understanding of the factors that determine the type of γ-brass cell and the ordering of the atoms therein. Placing the larger In atoms in *BOH*

and *BCO* maximizes the packing fraction (Fig. 1) and we assumed an *I* cell since the packing-fraction calculations were carried out for this cell, it being too complicated to attempt the calculation for a *P* cell. In fact, going from the *I* cell to the *P* cell reduces the number of contacts for the large In atoms with themselves and increases the number of unlike In–Mn contacts as Table 7 shows (the same was shown to be true at a composition M_4N_9; Brandon, Brizard, Pearson & Tozer, 1977) and both of these effects further increase the stability of the structure. Hence it is not surprising that $InMn_3$ has a *P* rather than an *I* cell, a point which we did not consider at the time of our predictions. Nevertheless, the new type of ordering was correctly predicted for $InMn_3$.

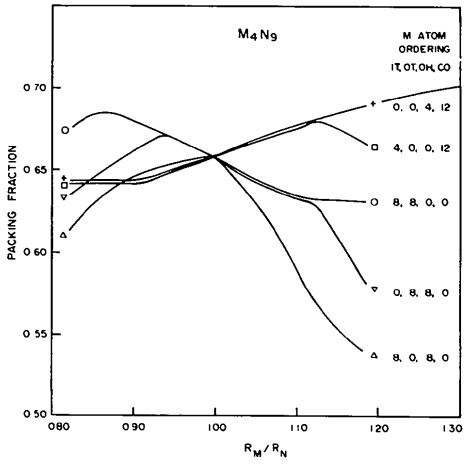

Fig. 1. Packing fraction calculated as a function of radius ratio for γ-brasses with the *I* cell at a composition M_4N_9. At large radius ratios the packing fraction is improved by ordering the larger atoms in *OH* and *CO* sites.

(*d*) *Re-evaluation of Reynolds's high-temperature powder data for* γ-Cu–In

The discovery of a unique atomic ordering and a *P* cell for the γ-In–Mn phase led us to examine the possibility that the high-temperature γ-Cu–In powder diffraction data (Reynolds, 1952) might be consistent with a *P* cell and with the $InMn_3$ type of atomic ordering which has larger In atoms in *CO* and *OH* sites of one cluster. Indeed, if the γ-Cu–In data were not consistent with such a model, one would be faced with the problem of understanding why γ-In–Mn and γ-Cu–In were different with practically the same radius ratio.

Reynolds's original powder intensity data are contained in Table 8 along with the values of $N = h^2 + k^2$

Table 7. *Ordering of M atoms and number of neighbours per cell for a selection of M_xN_y structures with I or P cells*

Number	$x:y$	Cell type	Ordering of *M* atoms	Weighted number of neighbours per cell *M–M*	*N–N*	*M–N*	Average number of *M–N* contacts per *M* atom
1	16:36	*P*	4 in *AIT* 12 in *BCO*	6	102	150	9·38
2			4 in *BOH* 12 in *BCO*	$9\frac{1}{3}$	$117\frac{1}{3}$	$131\frac{1}{3}$	8·21
3	13:39	*P*	1 in *AIT* 12 in *BCO*	$\frac{3}{8}$	$132\frac{3}{8}$	$125\frac{1}{4}$	9·63
4			4 9	6	$130\frac{1}{2}$	$121\frac{1}{2}$	9·35
5	13:39	*I*	4 in *OH* 9 in *CO*	$14\frac{11}{12}$	$151\frac{5}{12}$	$91\frac{2}{3}$	7·05
6			2 11	$14\frac{5}{6}$	$150\frac{1}{3}$	$92\frac{5}{6}$	7·14
7			0 13	$14\frac{1}{12}$	$148\frac{7}{12}$	$95\frac{1}{3}$	7·33
8	13:39	*P*	1 in *BOH* 12 in *BCO*	$2\frac{1}{12}$	$137\frac{1}{12}$	$118\frac{5}{6}$	9·14
9			2 11	4	$139\frac{1}{2}$	$114\frac{1}{2}$	8·81
10			3 10	$5\frac{3}{4}$	$141\frac{3}{4}$	$110\frac{1}{2}$	8·50
11			4 9	$7\frac{1}{3}$	$143\frac{5}{6}$	$106\frac{5}{6}$	8·22
12			5 8	$8\frac{3}{4}$	$145\frac{3}{4}$	$103\frac{1}{2}$	7·96
13			6 7	10	$147\frac{1}{2}$	$100\frac{1}{2}$	7·73

$+ l^2$ adopted in the cubic indexing. These measurements were obtained from a sample containing 29·6 at.% In exposed to Ni-filtered Cu radiation at 923 K in a 190 mm Unicam high-temperature camera. Reynolds noted four extra lines which could be assigned N values for the Cu $K\bar{\beta}$ wavelength. These same N values (18, 36, 46 and 48) matched up with 'strong' or 'medium strong' lines for the Cu $K\bar{\alpha}$ wavelength and the explanation for these four extra lines in the cubic powder-pattern indexing is quite acceptable. Among all the remaining lines, two classed as 'very weak' require odd values of N (9 and 129) to fit the cubic indexing. These two very weak lines might now indeed be seen as evidence of a primitive cubic lattice (P cell) for γ-Cu–In since the archetype I cell could only produce lines with N even.

A computer program was written to calculate powder diffraction line intensities $I_c(N)$ for cubic γ-brass-type structure models. The usual structure factor calculations were made for a model structure and inverse Lorentz and polarization factors were applied in order to generate calculated intensities which could be compared to Reynolds's visual estimates from films. Multiplicity factors were assigned for the different classes of hkl values concerned and intensities were added for superposed powder lines. The resulting $I_c(N)$ were scaled onto a range from 0 to 100. In the calculation of structure factors, an overall temperature factor B_o was treated as an adjustable parameter of the model structure. From experience, agreement was improved between calculated and observed powder intensities at both high and low scattering angles when B_o was negative, suggesting that considerable absorption was present in the observed data. This finding is consistent with Reynolds's remarks concerning observed shifts in line positions attributed to absorption in the sample. We were not able to apply realistic inverse absorption corrections without more details of experimental conditions such as sample size *etc.*, so we chose instead to allow B_o to become negative if necessary to partially compensate for lower observed relative intensities at low angles due to absorption.

Powder line intensities $I_c(N)$ were then calculated for allowed cubic N values from 1 to 134 for a P-cell model with composition In_4Cu_9 (30·77 at.% In) and with 12 In in BCO, 2 in BOH and 2 in AOH. Coordinates like those for γ-$InMn_3$ in Table 3 were used and B_o was set $\sim -0{\cdot}2$ Å^2. The results appear in Table 8. Among all the N-odd lines, $I_c(9) = 5{\cdot}6$ was the largest (greater than the second largest by a factor of ~2) and it corresponds

Table 8. *High-temperature powder diffraction line intensities as observed and as calculated for* γ-Cu–In *models*

N (even)	I_o*	I_c $InMn_3$ type	I_c Cu_9Al_4 type	N (odd)	I_o*	I_c $InMn_3$ type	I_c Cu_9Al_4 type	N (even)	I_o*	I_c $InMn_3$ type	I_c Cu_9Al_4 type	N (odd)	I_o*	I_c $InMn_3$ type	I_c Cu_9Al_4 type
2		0·2	0·3	1		0·5	0·7	68		1·3	0·8	69		0·1	0·4
4		0·1	0·8	3		1·6	0·2	70		0·0	1·0				
6		0·8	1·0	5		2·7	0·8	72	*m*	2·6	1·9	73		0·5	0·6
8		0·4	0·9	9	*vw*	5·6	14·1	74		0·9	0·8	75		0·2	0·0
10		2·6	0·0	11		0·8	0·0	76		1·3	2·3	77		0·2	0·3
12	*w*	8·5	13·3	13		0·2	0·3	78		1·3	1·0				
14	*w*	8·5	6·7					80		0·0	0·5	81		0·6	0·7
16		0·5	0·0	17		1·3	1·4	82		0·6	0·5	83		0·0	0·3
18	*vs*	96·3	92·5	19		0·5	0·7	84		0·4	0·3	85		0·1	0·0
20		1·3	1·0	21		0·1	0·2	86		0·9	0·3				
22	*m*	6·3	6·9	25		0·5	0·5	88		0·5	0·5	89		0·4	1·2
24		3·1	1·3	27		0·7	1·7	90	*w*	2·2	0·7	91		0·1	0·5
26	*w*	3·6	3·6	29		0·3	0·2	94		0·4	0·9	93		0·1	0·1
30	*w*	2·0	5·1					96		0·3	0·3	97		0·1	0·4
32		0·1	0·9	33		1·7	3·1	98	*w*	3·7	3·9	99		0·3	0·3
34		1·6	0·9	35		0·5	0·1	100		0·4	0·4	101		0·2	0·4
36	*m*	6·1	6·1	37		0·0	0·0	102	*w*	1·5	1·7				
38		3·1	1·1					104		0·7	0·5	105		0·4	0·5
40		0·0	0·0	41		0·7	1·0	106		0·8	0·6	107		0·2	0·0
42		0·3	0·2	43		0·2	0·3	108	*w*	2·5	2·3	109		0·0	0·5
44	*m*	1·0	0·3	45		0·2	0·2	110		1·2	1·2	113		0·3	0·9
46	*m*	3·3	4·2					114	*ms*	5·9	4·8	115		0·2	0·2
48	*m*	4·8	4·7	49		0·5	1·3	116		0·2	0·3	117		0·1	0·2
50	*vw*	2·7	3·3	51		0·3	0·8	118		1·6	2·9				
52		0·7	0·3	53		0·1	0·1	120	*w*	2·0	1·6	121		0·5	1·3
54	*s*	14·7	13·5					122		1·3	1·2	123		0·0	0·3
56		0·9	0·6	57		0·3	0·3	126	*ms*	8·9	5·9	125		0·1	0·1
58		0·8	0·4	59		0·2	0·5	128	*w*	2·5	2·9	129	*vw*	1·2	2·0
62		1·9	1·2	61		0·2	0·3	130		1·2	0·8	131		0·2	0·4
64		0·4	0·2	65		0·3	0·7	132	*w*	2·3	2·2	133		0·1	0·1
66	*ms*	6·7	7·8	67		0·0	0·0	134	*w*	3·8	3·7				

* Visually estimated intensities as assigned by Reynolds (1952): *vs* = very strong; *s* = strong; *ms* = medium strong; *m* = medium; *w* = weak; *vw* = very weak.

to one of the two observed lines in Reynolds's data that required N odd for cubic indexing. $I_c(129) = 1{\cdot}2$ is the largest calculated value in the high-angle region for N odd (the sixth-largest N-odd line in the entire pattern) and it corresponds to the other N-odd line recorded by Reynolds. Other N-odd lines with $I_c(N)$ values between these two [$I_c(5) = 2{\cdot}7$, $I_c(33) = 1{\cdot}7$, $I_c(3) = 1{\cdot}6$, $I_c(17) = 1{\cdot}3$] were not observed by Reynolds presumably because they occur in the forward scattering region where absorption effects are larger and the threshold of observability corresponds to larger I_c values. As examples which are consistent with this presumption we see (i) that $N = 9$ at 5·6 in the low-angle region and $N = 129$ at 1·2 in the high-angle are both just barely observable and have the same 'very weak' label, (ii) that low-angle $N = 12$ at 8·5 and some six high-angle lines with $N > 100$ at an average 2·4 all have the same 'weak' label, and (iii) that the low-angle $N = 10$ line at 2·6 falls below the low-angle observability threshold. When considering agreement for N-even lines we find $N = 18$ at 96·3 matching the strongest observed line. Minor discrepancies remain such as why lines $N = 24$ and 38 were not observed whereas line $N = 30$ was, but this variation among generally weak lines which do calculate as weak is not of too great concern.

The very low value $I_c(44) = 1{\cdot}0$ which Reynolds classified as 'medium' appears to be a more serious deficiency. However, we can explain it as a Cu $K\bar{\beta}$ component associated with the second-strongest line in the pattern which was indexed as $N = 54$ for the Cu $K\alpha_1$ wavelength.* This β assignment was not noticed by Reynolds because the $N = 44$ choice happens to adequately match the Cu $K\bar{\alpha}$ wavelength. Our model for the structure leads us to suggest instead that this should be interpreted as a β line, and the very small calculated $I_c(44)$ value is no longer inconsistent with the observations. The observation of line $N = 102$ when $I_c(102)$ calculates rather small can similarly be explained as a β component arising from the 'medium strong' $N = 126$ line.

Thus it is a fair interpretation that γ-Cu–In does indeed have a P cell like γ-$InMn_3$, and calculated intensities for $InMn_3$-type ordering of the In and Cu atoms are not inconsistent with the intensities reported by Reynolds (1952) subject to the remarks above. Whether this ordering gives significantly better agreement than Al_4Cu_9-type ordering is difficult to say with the visually estimated data available. One may cite, however, that I_{obs} and $I_c(N)$ for the low-angle reflections $N = 9$, 12 and 14 would favour the model with $InMn_3$ rather than Al_4Cu_9 type of ordering (Table 8).

* The $K\alpha_1$ to $K\bar{\beta}$ wavelength ratio 1·54056/1·39222 = 1·1066 is matched well by the ratio of sines for the reported θ angles sin (37·999°)/sin (33·853°) = 1·1052.

This work was made possible through financial support provided by the National Research Council of Canada. One of the authors (HSK) gratefully acknowledges scholarship support from the University of Waterloo. We are also grateful to Dr J. W. Christian FRS, for supplying a copy of Reynolds's diffraction data for the γ-Cu–In phase.

References

AOYAGI, K. & SUGIHARA, M. (1962). *J. Phys. Soc. Jpn*, **17**, 1072–1073.

ARNBERG, L. & WESTMAN, S. (1978). *Acta Cryst.* A**34**, 399–404.

BOOTH, M. H., BRANDON, J. K., BRIZARD, R. Y., CHIEH, C. & PEARSON, W. B. (1977). *Acta Cryst.* B**33**, 30–36.

BRANDON, J. K., BRIZARD, R. Y., CHIEH, P. C., MCMILLAN, R. K. & PEARSON, W. B. (1974). *Acta Cryst.* B**30**, 1412–1417.

BRANDON, J. K., BRIZARD, R. Y., PEARSON, W. B. & TOZER, D. J. N. (1977). *Acta Cryst.* B**33**, 527–537.

BRANDON, J. K., PEARSON, W. B., RILEY, P. W., CHIEH, C. & STOKHUYZEN, R. (1977). *Acta Cryst.* B**33**, 1088–1095.

HANSEN, M. (1958). *Constitution of Binary Alloys*, 2nd ed., pp. 850–852. New York: McGraw-Hill.

HEIDENSTAM, O. VON, JOHANSSON, A. & WESTMAN, S. (1968). *Acta Chem. Scand.* **22**, 653–661.

International Tables for X-ray Crystallography (1968). Vol. III, 2nd ed., pp. 210–216. Birmingham: Kynoch Press.

International Tables for X-ray Crystallography (1969). Vol. I, 3rd ed., pp. 316, 324, 330. Birmingham: Kynoch Press.

KIM, H. S. (1979). PhD Thesis, Univ. of Waterloo (to be published).

PEARSON, W. B., BRANDON, J. K. & BRIZARD, R. Y. (1976). *Z. Kristallogr.* **143**, 387–416.

REYNOLDS, J. (1952). Thesis, Oxford Univ., pp. 84–92.

STOKHUYZEN, R., BRANDON, J. K., CHIEH, P. C. & PEARSON, W. B. (1974). *Acta Cryst.* B**30**, 2910–2911.

WESTMAN, S. (1965). *Acta Chem. Scand.* **19**, 1411–1419.

ZWICKER, U. (1950). *Z. Metallkd.* **41**, 399–400.